mathematics

MDPI

Article

Detecting Line Sources inside Cylinders by Analytical Algorithms

Dimitrios S. Lazaridis † and Nikolaos L. Tsitsas *,†

School of Informatics, Aristotle University of Thessaloniki, 54124 Thessaloniki, Greece; lazdimspy@csd.auth.gr
* Correspondence: ntsitsas@csd.auth.gr
† These authors contributed equally to this work.

Abstract: Inverse problems for line sources radiating inside a homogeneous magneto-dielectric cylinder are investigated. The developed algorithms concern the determination of the location and the current of each source. These algorithms are mostly analytical and are based on proper exploitation of the moments obtained by integrating the product of the total field on the cylindrical boundary with complex exponential functions. The information on the unknown parameters of the problem is encoded in these moments, and hence all parameters can be recovered by means of relatively simple explicit expressions. The cases of one and two sources are considered and analyzed. Under certain conditions, the permittivity and permeability of the cylinder are also recovered. The results from two types of numerical experiments are presented: (i) for a single source, the effect of noise on the boundary data is studied, (ii) for two sources, the pertinent nonlinear system of equations is solved numerically and the accuracy of the derived solution is discussed.

Keywords: line sources; inverse scattering; cylinders; analytical algorithms

MSC: 78A46; 35Q60; 35Q61

Citation: Lazaridis, D.S.; Tsitsas, N.L. Detecting Line Sources inside Cylinders by Analytical Algorithms. *Mathematics* **2023**, *11*, 2935. https://doi.org/10.3390/math11132935

Academic Editor: Panayiotis Vafeas

Received: 22 May 2023
Revised: 21 June 2023
Accepted: 25 June 2023
Published: 30 June 2023

1. Introduction

Identifying point sources or point dipoles inside an object using field measurements on its boundary is a classic example of an *inverse-source problem* [1]. In this work, we consider two-dimensional (2-D) inverse line-source problems in which we seek to determine the locations and currents of one or two electric-current filaments located inside a homogeneous and isotropic magneto-dielectric cylindrical medium. Electromagnetic inverse problems of this type may find applications in biomedical diagnostics related to the operation principles of microwave tomographic systems [2,3], and in microwave detection and positioning of dielectric scatterers and pipes inside an enclosure [4] as well as in the detection of cavities in tree trunks [5,6]. We use as measurements the values of the electric field on the boundary of the medium. Then, we calculate the moments obtained by integrating the product of the total field on the cylindrical boundary with complex exponential functions; these are suitable normalized Fourier coefficients of the boundary data. The unknown parameters of the problem can be determined explicitly by means of these moments. In the case of a single internal source, the location coordinates and the current of the source as well as (under certain conditions) the permittivity and permeability of the medium are determined explicitly. For two internal sources, the medium's characteristics are considered as known and we determine the location coordinates and currents of both sources.

Moreover, we present numerical results for both problems referring to one or two line sources. First, for a single source, we analyze the effect of noisy boundary data on the determination of the unknown parameters. It is seen that the only parameter that is affected by the noise in the measurements is the current of the source. Then, it is shown that the relative error in the determination of the current increases with the noise level (as expected);

however, it remains in acceptable levels and well below its upper bound. Next, for two sources, we solve numerically the nonlinear system involving the associated unknown parameters by using a nonlinear least-squares method. The parameters are computed accurately provided that the initial values do not have large deviations from the true ones; a detailed comparative analysis for all parameters is included. Furthermore, in the low-frequency regime, we solve explicitly the pertinent system of equations. Performing a related numerical investigation, we find that for $k_0 a \leq 0.01$ (a is the radius of the cylinder and k_0 is the free-space wavenumber), the parameters of the two sources are computed with negligible error.

Numerical schemes for treating 2-D inverse-source problems in electrostatics and magnetostatics were devised in [7–11]. Precisely, in [7], inverse problems were investigated for locating point-wise or small-size conductivity defaults in planar domains from overdetermined boundary measurements of solutions to Laplace's equation. In [8], inverse problems were analyzed concerning sources detection from boundary data in a 2-D medium with piece-wise constant conductivity by using the best rational or harmonic approximations in specific domains. Furthermore, in [9], a reciprocity-gap principle method was developed for locating point sources in planar domains from overdetermined boundary measurements of solutions of Poisson's equation. In [10], steady-state electrostatic or thermal imaging boundary-value problems for Laplace's equation were considered and algorithms were proposed for determining the compact support of inclusions by solving a simpler equivalent point-source problem. In [11], inverse problems in the 2-D Helmholtz equation from Cauchy data were considered concerning the determination of point-wise sources and sources having compact support within a finite number of small subdomains.

On the other hand, regarding three-dimensional (3-D) inverse-source problems, finding an electrostatic or an acoustic point source inside a homogeneous sphere by using appropriate moments on the spherical boundary was investigated in [12]. Conventional and reciprocal approaches based on forward-transfer matrices were employed in [13] to obtain single-dipole solutions on spherical boundary-element model using simplex optimization. In [14], inverse-source problems for the 3-D time-harmonic Maxwell's equations were studied by using boundary measurements of the radiated fields and formulating a system of integro-differential equations. In [15], recovering acoustic monopoles was investigated by means of point-wise acoustic-pressure measurements at a limited number of frequencies and formulation of associated sparse optimization problems for the Helmholtz equation. Besides, determining characteristic sources in the modified and classical Helmholtz equations based on external boundary measurements and a minimization scheme for an equivalent reciprocity functional was analyzed in [16]. In [17], three reconstruction algorithms were proposed for the Helmholtz equation, using near-field Cauchy data on the external boundary, to detect the number, location, size, and shape of hidden sources. An algebraic algorithm to identify the number, locations and intensities of the point sources from boundary measurements for the Helmholtz equation in an interior domain was developed in [18]. An iterative method for numerical reconstruction of the unknown source function in Poisson's and Helmholtz equations by means of measurements collected at the boundary was presented in [19]. In [20], linear integral transforms in Hilbert spaces were introduced and inversion formulas for inverse-source problems in the Helmholtz equation were provided. In the context of brain imaging, inverse problems for point sources or dipoles inside spheres or ellipsoids were presented and discussed in [21,22].

This paper is organized as follows. In Section 2, we formulate the direct scattering problem due to a single internal line source and present its exact solution. In Section 3, we solve the pertinent inverse line-source problem either when the cylinder has a known refractive index or when the cylinder is electrically small. The case of two internal line sources is analyzed in Section 4. Several numerical results for a single line source or for two line sources are presented in Section 5. Particularly, the effect of noisy boundary data on the determination of the unknown parameters of a single line source is analyzed in

Section 5.1. Moreover, in Section 5.2, we consider the case of two line sources and examine the sensitivity in the determination of the involved parameters with respect to the variations of their respective initial values. The paper closes with conclusions in Section 6.

2. The Direct Problem and Its Exact Solution

An infinite along the z-axis circular magneto-dielectric cylinder of radius a, with relative dielectric permittivity ϵ_1 and magnetic permeability μ_1 lies in free space with permittivity ϵ_0 and permeability μ_0. The cylinder is excited by an internal z-directed electric-current filament I, located at $(\rho, \phi) = (h, \phi_0)$, with $h < a$.

The sole z-component of the primary electric field $\mathbf{E}^{\rm pr}(\rho, \phi) = E^{\rm pr}(\rho, \phi)\hat{\mathbf{z}}$ is given by (under $\exp(-\mathrm{i}\omega t)$ time dependence, with ω as the angular frequency and t as time)

$$E^{\rm pr}(\rho, \phi) = A\, I\, H_0\left(k_1\sqrt{\rho^2 + h^2 - 2\rho h\cos(\phi - \phi_0)}\right),$$

where H_n denotes the n-th order cylindrical Hankel functions of the first-kind $H_n^{(1)}$, while $k_0 = \omega\sqrt{\epsilon_0\mu_0}$ and $k_1 = k_0 n_1$ are the external and internal wavenumbers, respectively, with $n_1 = \sqrt{\epsilon_1\mu_1}$ being the refractive index of the cylinder, and $A = -(\omega\mu_0\mu_1)/4$.

The total electric field in the interior of the cylinder is expressed as

$$E_1(\rho, \phi) = E^{\rm pr}(\rho, \phi) + E^{\rm sec}(\rho, \phi), \quad 0 < \rho < a, \quad (\rho, \phi) \neq (h, \phi_0),$$

where $E^{\rm sec}$ is the generated secondary electric field.

Imposing the boundary conditions referring to the continuity of the tangential components of the electric and magnetic fields on $\rho = a$, we obtain the following exact expressions of the z-components of the total electric field outside the cylinder and the secondary electric field inside the cylinder [23]

$$E_0(\rho, \phi) = A\, I \sum_{n=-\infty}^{\infty} \alpha_n H_n(k_0\rho) e^{\mathrm{i}n(\phi - \phi_0)}, \quad \rho > a,$$

$$E^{\rm sec}(\rho, \phi) = A\, I \sum_{n=-\infty}^{\infty} \beta_n J_n(k_1\rho) e^{\mathrm{i}n(\phi - \phi_0)}, \quad 0 < \rho < a,$$

where

$$\alpha_n = -\frac{2\mathrm{i}}{a\pi}\frac{J_n(k_1 h)}{k_1 J_n'(k_1 a) H_n(k_0 a) - k_0\mu_1 H_n'(k_0 a) J_n(k_1 a)},$$

$$\beta_n = -J_n(k_1 h)\frac{k_1 H_n'(k_1 a) H_n(k_0 a) - k_0\mu_1 H_n'(k_0 a) H_n(k_1 a)}{k_1 J_n'(k_1 a) H_n(k_0 a) - k_0\mu_1 H_n'(k_0 a) J_n(k_1 a)},$$

with J_n denoting the n-th order cylindrical Bessel functions.

Now, the electric field on the cylinder (i.e., for $\rho = a$) is given by

$$E_{\rm cyl}(\phi) = E_0(a, \phi) = \tilde{A}\mu_1 I \sum_{n=-\infty}^{\infty} \alpha_n H_n(k_0 a) e^{\mathrm{i}n(\phi - \phi_0)},$$

where $\tilde{A} = -\omega\mu_0/4$, which is a known quantity for known angular frequency and free-space parameters.

This field $E_{\rm cyl}(\phi)$ is the basic function that we will use to find the line source and the internal parameters of the cylinder.

The above analysis refers to the excitation of the cylinder by a transverse magnetic (TM) polarized field with respect to the z-axis. In case of excitation by an internal z-directed magnetic-current filament I_M, the generated fields have transverse electric (TE) polarization, and the sole z-component of the magnetic field on $\rho = a$ is found to be [24]

$$H_{\text{cyl}}(\phi) = -\frac{\omega\epsilon_0\epsilon_1}{4} I_M \sum_{n=-\infty}^{\infty} \tilde{\alpha}_n H_n(k_0 a) e^{\mathrm{i}n(\phi-\phi_0)},$$

where

$$\tilde{\alpha}_n = -\frac{2\mathrm{i}}{a\pi} \frac{J_n(k_1 h)}{k_1 J_n'(k_1 a) H_n(k_0 a) - k_0 \epsilon_1 H_n'(k_0 a) J_n(k_1 a)}.$$

In the next sections, for simplicity, we examine only the case of TM polarization. The corresponding results for TE polarization are recovered by replacing μ_0 and μ_1 with ϵ_0 and ϵ_1, respectively, as well as I with I_M.

3. Inverse Line-Source Problem

We consider an inverse line-source problem in which we seek to determine the coordinates (h, ϕ_0) and the current I of the line source. Regarding the cylinder's material parameters ϵ_1 and μ_1, we will initially consider them as unknowns and see in which cases they can also be determined explicitly.

We define the normalized moments

$$M_n = \frac{1}{2\pi \tilde{A} H_n(k_0 a)} \int_{-\pi}^{\pi} E_{\text{cyl}}(\phi) e^{-\mathrm{i}n\phi} \mathrm{d}\phi = \mu_1 I \alpha_n e^{-\mathrm{i}n\phi_0}, \quad n \in \mathbb{Z}, \tag{1}$$

where the quantities $\tilde{A} H_n(k_0 a)$ used as normalization coefficients are known for known cylinder's radius a and free-space parameters.

First, we determine the angle ϕ_0 of the line source (without any assumptions on the parameters of the problem). Consider that $\alpha_1 = |\alpha_1| e^{\mathrm{i}\delta}$. Then, from (1) for $n = \pm 1$, and since $\mu_1 > 0$ and $I > 0$, we have that the complex number M_1 has the argument $\delta - \phi_0$ and the complex number $-M_{-1}$ has the argument $\delta + \phi_0$. Hence, both δ and ϕ_0 are determined.

3.1. Cylinder with Known Refractive Index

To make analytical progress, one option is to make some assumptions on the material parameters of the cylinder. Suppose that the refractive index n_1 is known, but ϵ_1 and μ_1 are unknown. We proceed to determine h, I, ϵ_1 and μ_1. Since $n_1 = \sqrt{\epsilon_1 \mu_1}$, if we find μ_1 then we can also determine ϵ_1.

From the recurrence relations of the cylindrical Bessel functions (Equation (9.1.27) of [25]), we have

$$\frac{1}{k_1 h} = \frac{J_{n-1}(k_1 h) + J_{n+1}(k_1 h)}{2n\, J_n(k_1 h)} = \frac{M_{n-1} d_{n-1} e^{-\mathrm{i}\phi_0} + M_{n+1} d_{n+1} e^{\mathrm{i}\phi_0}}{2n\, M_n d_n}, \quad n \geq 1, \tag{2}$$

where

$$d_n = k_1 J_n'(k_1 a) H_n(k_0 a) - k_0 \mu_1 H_n'(k_0 a) J_n(k_1 a). \tag{3}$$

Next, equating two of (2), yields

$$\frac{M_{n-1} d_{n-1} e^{-\mathrm{i}\phi_0} + M_{n+1} d_{n+1} e^{\mathrm{i}\phi_0}}{n\, M_n d_n} = \frac{M_n d_n e^{-\mathrm{i}\phi_0} + M_{n+2} d_{n+2} e^{\mathrm{i}\phi_0}}{(n+1) M_{n+1} d_{n+1}},$$

which takes the form

$$(n+1) M_{n+1} d_{n+1} \left(M_{n-1} d_{n-1} + M_{n+1} d_{n+1} e^{2\mathrm{i}\phi_0} \right) = n M_n d_n \left(M_n d_n + M_{n+2} d_{n+2} e^{2\mathrm{i}\phi_0} \right).$$

Since d_n is linear in μ_1 (for known n_1), the last is a quadratic equation for μ_1, for each $n \geq 1$. This equation is written as

$$A_n \mu_1^2 + B_n \mu_1 + C_n = 0, \tag{4}$$

where

$$\begin{aligned}
A_n =&(n+1)M_{n+1}^2 e^{2i\phi_0}\left[k_0 H_{n+1}'(k_0a)J_{n+1}(k_1a)\right]^2\\
&+(n+1)M_{n+1}M_{n-1}\Big[k_0^2 H_{n-1}'(k_0a)J_{n-1}(k_1a)\\
&H_{n+1}'(k_0a)J_{n+1}(k_1a)\Big]-nM_n^2\left[k_0 H_n'(k_0a)J_n(k_1a)\right]^2\\
&-nM_nM_{n+2}e^{2i\phi_0}\left[k_0^2 H_n'(k_0a)J_n(k_1a)H_{n+2}'(k_0a)J_{n+2}(k_1a)\right],\\
B_n =&nM_n^2\left[2k_0k_1J_n'(k_1a)H_n(k_0a)H_n'(k_0a)J_n(k_1a)\right]\\
&+nM_nM_{n+2}e^{2i\phi_0}k_0k_1\Big[J_n'(k_1a)H_n(k_0a)H_{n+2}'(k_0a)\\
&J_{n+2}(k_1a)+J_{n+2}'(k_1a)H_{n+2}(k_0a)H_n'(k_0a)J_n(k_1a)\Big]\\
&-(n+1)M_{n+1}^2e^{2i\phi_0}\Big[2k_0k_1J_{n+1}'(k_1a)H_{n+1}(k_0a)\\
&H_{n+1}'(k_0a)J_{n+1}(k_1a)\Big]-(n+1)M_{n+1}M_{n-1}k_0k_1\\
&\Big[J_{n-1}'(k_1a)H_{n-1}(k_0a)H_{n+1}'(k_0a)J_{n+1}(k_1a)\\
&+J_{n+1}'(k_1a)H_{n+1}(k_0a)H_{n-1}'(k_0a)J_{n-1}(k_1a)\Big],\\
C_n =&(n+1)M_{n+1}^2e^{2i\phi_0}\left[k_1J_{n+1}'(k_1a)H_{n+1}(k_0a)\right]^2\\
&+(n+1)M_{n+1}M_{n-1}k_1^2J_{n-1}'(k_1a)H_{n-1}(k_0a)\\
&J_{n+1}'(k_1a)H_{n+1}(k_0a)-nM_n^2\left[k_1J_n'(k_1a)H_n(k_0a)\right]^2\\
&-nM_nM_{n+2}e^{2i\phi_0}k_1^2J_n'(k_1a)H_n(k_0a)J_{n+2}'(k_1a)H_{n+2}(k_0a).
\end{aligned}$$

The relative permeability μ_1 solves (4), for each $n \geq 1$. Having determined μ_1, the coordinate h of the source's location is found using (2). Then, the relative permittivity ϵ_1 follows from the definition of n_1. The current I is finally obtained from the moments M_n given by (1).

3.2. Electrically-Small Cylinder

If the refractive index n_1 is unknown, then we can derive explicit expressions for the problem's parameters pertaining to an electrically-small cylinder, i.e., when we are in the low-frequency regime [26]. Precisely, for $k_0a \ll 1$ and $k_1a \ll 1$, the coefficients α_n have the following leading-order low-frequency approximations, as $k_0a \to 0$ and $k_1a \to 0$,

$$\alpha_0 \sim \frac{1}{\mu_1}, \quad \alpha_n \sim \frac{(k_0h)^n}{2^{n-1}n!(1+\mu_1)}, \; n \geq 1. \tag{5}$$

Combining the latter with (1), gives

$$\frac{4M_2e^{i\phi_0}}{k_0M_1} = \frac{4\alpha_2}{k_0\alpha_1} = h,$$

which determines h. Subsequently, the current I of the line source is obtained by

$$M_0 = \mu_1 I\alpha_0 = I.$$

Then, the relative permittivity μ_1 is found by

$$\frac{M_1}{Ik_0he^{-\mathrm{i}\phi_0} - M_1} = \mu_1.$$

However, we cannot determine the refractive index n_1, and therefore ϵ_1, from the leading-order approximations (5) of α_n, because n_1 (or alternatively the wavenumber k_1) does not appear. To this end, we could use a higher-order low-frequency approximation, like, e.g.,

$$\alpha_0 \sim \frac{1 - \frac{1}{4}(k_1h)^2}{(k_1a)^2\left(-\frac{1}{2}(k_0a)^2 + 2k_0a - \frac{3}{2}\right) + \mu_1\left(1 - \frac{1}{4}(k_1a)^2\right)},$$

by which we obtain an estimate for k_1, and hence for n_1 and ϵ_1.

4. The Case of Two Internal Line Sources

Now, we consider that there are two line sources inside the magneto-dielectric cylinder with unknown electric-current filaments I_1 and I_2, and unknown position vectors $(\rho, \phi) = (h_1, \phi_1)$ and $(\rho, \phi) = (h_2, \phi_2)$, respectively. The cylinder's material parameters ϵ_1 and μ_1 are supposed to be known.

By linear superposition and the definition (1) of the moments, we get

$$M_n = -\frac{2\mathrm{i}}{a\pi}\frac{\mu_1}{d_n}\left(I_1J_n(k_1h_1)e^{-\mathrm{i}n\phi_1} + I_2J_n(k_1h_2)e^{-\mathrm{i}n\phi_2}\right), \quad n \in \mathbb{Z}, \tag{6}$$

where d_n, given by (3), is known for known parameters of the cylinder.

We can proceed analytically in the low-frequency regime, i.e., assuming that $k_0a \ll 1$ and $k_1a \ll 1$. Then, by (5), we obtain, as $k_0a \to 0$ and $k_1a \to 0$,

$$M_0 \sim I_1 + I_2, \qquad M_n \sim \gamma_n\left(I_1h_1^ne^{-\mathrm{i}n\phi_1} + I_2h_2^ne^{-\mathrm{i}n\phi_2}\right), \quad n \geq 1, \tag{7}$$

where

$$\gamma_n = \frac{\mu_1k_0^n}{2^{n-1}n!(1+\mu_1)}.$$

If $\phi_1 = \phi_2 = \phi_0$ then we can determine ϕ_0 from M_1. From (7), we have

$$\frac{M_1}{\gamma_1} \sim (I_1h_1 + I_2h_2)e^{-\mathrm{i}\phi_0}.$$

Since $I_1h_1 + I_2h_2 > 0$, the complex number $\frac{M_1}{\gamma_1}$ has the argument $-\phi_0$.

Now, the other unknown parameters I_1, I_2, h_1 and h_2 are found by means of the moments M_0, M_1, M_2 and M_3 as follows:

$$h_1 = \frac{\tilde{M}_1\tilde{M}_2 - \tilde{M}_0\tilde{M}_3 + \sqrt{\left(\tilde{M}_1\tilde{M}_2 - \tilde{M}_0\tilde{M}_3\right)^2 + 4\left(\tilde{M}_1^2 - \tilde{M}_0\tilde{M}_2\right)\left(-\tilde{M}_2^2 + \tilde{M}_1\tilde{M}_3\right)}}{2\left(\tilde{M}_1^2 - \tilde{M}_0\tilde{M}_2\right)}, \tag{8}$$

$$h_2 = \frac{\tilde{M}_1\tilde{M}_2 - \tilde{M}_0\tilde{M}_3 - \sqrt{\left(\tilde{M}_1\tilde{M}_2 - \tilde{M}_0\tilde{M}_3\right)^2 + 4\left(\tilde{M}_1^2 - \tilde{M}_0\tilde{M}_2\right)\left(-\tilde{M}_2^2 + \tilde{M}_1\tilde{M}_3\right)}}{2\left(\tilde{M}_1^2 - \tilde{M}_0\tilde{M}_2\right)}, \tag{9}$$

$$I_1 = \frac{\tilde{M}_1 - h_2\tilde{M}_0}{h_1 - h_2}, \tag{10}$$

$$I_2 = \tilde{M}_0 - I_1, \tag{11}$$

where

$$\tilde{M}_n = \frac{M_ne^{\mathrm{i}n\phi_0}}{\gamma_n}, \quad n \geq 1$$

are known quantities.

5. Numerical Results and Discussion

5.1. Single Line Source

First, we consider the case of a single internal line source and present results of numerical experiments when the boundary data are measured in the presence of increasing levels of noise. Precisely, we consider that the measured electric field on $\rho = a$ is given by

$$E^{\delta}_{\mathrm{cyl}}(\phi) = N_{\delta} E_{\mathrm{cyl}}(\phi),$$

where $E_{\mathrm{cyl}}(\phi)$ is the true field on $\rho = a$, and N_{δ} is the noise function, which has the form

$$N_{\delta} = 1 + \delta \, rand.$$

with δ being noise-level parameter, while the function *rand* gives uniformly distributed random numbers in $[-1, 1]$.

Now, from (1), we see that the noise is inherited from E_{cyl} directly to the moments M_n, namely, it holds that the noisy moments are given by

$$M^{\delta}_{n} = N_{\delta} M_{n}.$$

Importantly, the only unknown parameter that is affected by the noise in the measurements is the current I. This is because I is determined directly from the noisy moments M^{δ}_{n} via (1). On the other hand, the other unknown parameters of the problem are determined by means of ratios of the noisy moments, and thus, the contribution of the noise is eliminated.

Let the noisy estimate for the true current I be denoted by $I_{\delta} = N_{\delta} I$. Then, for the relative error of the determination of I, holds

$$e(\delta) \equiv \frac{|I - I_{\delta}|}{|I|} \leqslant \delta. \tag{12}$$

We add noise to the electric-field boundary data with the noise level δ ranging from 2% to 20% with a step of 2%. The values of the current I obtained by implementing the analytic algorithm of Section 3.1 in the presence of the aforementioned noisy data are shown in Tables 1 and 2, corresponding to the cases of $I = 2$ and $I = 5$, respectively. For each case, ten iterations for the random noise were simulated (for each constant value of δ). We used Matlab R2017a for deriving the numerical results and performing the subsequent visualizations.

Table 1. Determined noisy values I^{δ} for different noise levels δ. The true value of the line-source's current is $I = 2$. The other parameters of the problem are $k_0 a = 2, k_0 h = 1, n_1 = 2, \mu_1 = 3, \phi_0 = \pi/4$.

δ%	Number of Iterations for the Random Noise									
	1	**2**	**3**	**4**	**5**	**6**	**7**	**8**	**9**	**10**
2	2.0098	2.0070	1.9766	1.9841	1.9977	1.9784	2.0275	1.9756	1.9781	1.9737
4	1.9564	1.9897	1.9698	2.0677	1.9888	1.9496	2.0648	2.0768	1.9902	1.9378
6	1.9419	1.9781	2.0228	1.9429	2.0247	2.0507	1.9332	1.9082	1.9512	1.9565
8	1.9757	2.0025	1.8674	1.9240	2.0963	1.8494	2.1372	2.0737	1.9964	2.0251
10	1.8949	1.9835	2.1852	2.0187	2.0085	1.8926	1.9956	2.0496	2.0717	1.9582
12	1.9364	2.2342	1.7781	2.1849	2.1984	2.1422	1.8074	1.8857	1.9210	2.0863
14	1.7965	2.1239	1.7798	2.0861	1.9967	2.1563	2.1204	2.2261	2.2189	1.9071
16	2.1272	1.8066	1.6995	2.1562	2.0000	1.9872	2.2590	2.0703	2.0753	2.2300
18	2.2200	2.0552	1.7717	1.8128	2.2783	1.6606	1.9927	1.7609	2.3447	2.1531
20	2.0004	1.9769	1.6477	2.1456	1.6339	1.6572	2.0173	1.6774	2.2545	2.2540

Table 2. As in Table 1, but for true value of the line-source's current $I = 5$.

δ%	Number of Iterations for the Random Noise									
	1	**2**	**3**	**4**	**5**	**6**	**7**	**8**	**9**	**10**
2	5.0319	5.0037	5.0946	5.0298	5.0601	4.9908	4.9865	5.0651	4.9167	4.9266
4	4.8694	4.9564	5.1326	5.1213	4.8242	4.9597	5.0108	4.9667	5.0627	5.0512
6	4.8752	4.9590	4.7093	5.2904	4.8003	4.7637	4.9234	4.8189	4.9938	4.9037
8	5.3613	5.3363	4.6421	5.1903	4.8153	4.9383	5.0383	5.3542	4.9342	5.3864
10	4.8015	5.2011	5.1663	5.0391	5.1981	5.1665	4.6781	4.6280	5.4991	4.6711
12	4.4391	5.0734	5.4582	5.2030	4.6285	4.8427	4.9529	5.5780	4.5877	5.4266
14	5.2027	4.8268	4.5673	4.8996	4.9748	4.4689	5.1253	4.6167	4.8385	5.1162
16	4.6029	4.6647	5.1873	4.6244	5.5190	5.7723	5.3684	4.7502	5.1345	4.3724
18	5.7314	5.6834	5.5720	4.5693	5.1698	4.1405	4.8655	4.6629	4.3907	4.4218
20	4.8458	4.1885	5.1970	4.9418	5.3919	5.3998	5.2771	4.0672	4.1376	4.6392

Moreover, the average values of the relative error $e(\delta)$ (corresponding to the ten considered iterations) versus the noise level δ, as stemming from the data presented in Tables 1 and 2, are depicted in Figures 1 and 2, respectively. Evidently, the relative error increases with the noise level. However, it remains well below its upper bound specified according to (12); the red line $e(\delta) = \delta$ in Figures 1 and 2 corresponds to that bound. In fact, the distance between the obtained error $e(\delta)$ and its upper bound δ generally increases with increasing δ. Specifically, the error $e(\delta)$ reaches at most 10% for noise levels δ up to 20%, while $e(\delta)$ remains smaller than 5% for δ up to 10%.

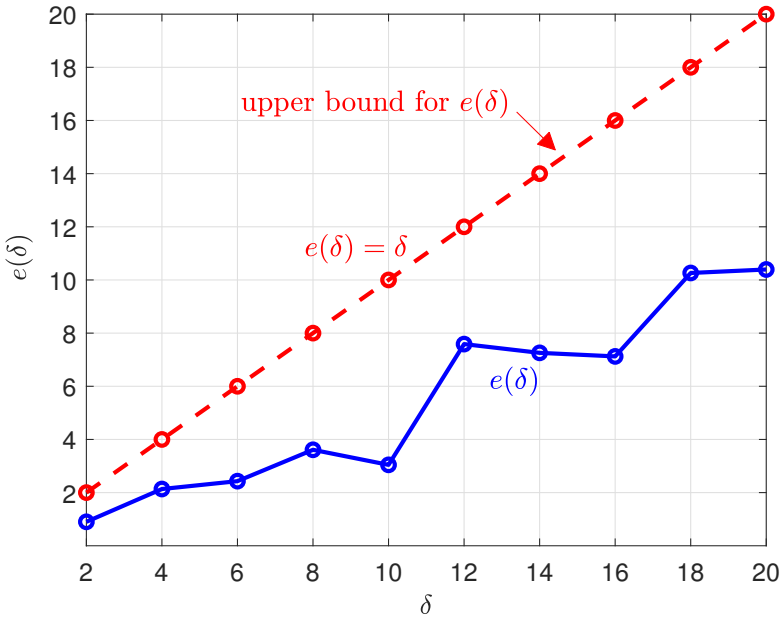

Figure 1. Average values of the relative errors $e(\delta)$ versus the noise level δ for the ten considered iterations of the random noise. The line $e(\delta) = \delta$ specifying the upper bound of the relative errors, according to (12), is also depicted. The true value of the line-source's current is $I = 2$.

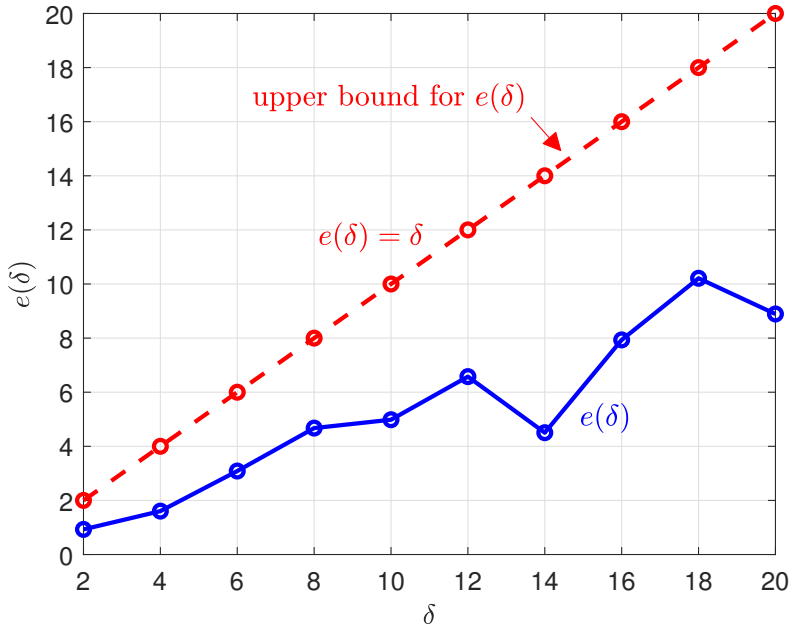

Figure 2. As in Figure 1, but for true value of the line-source's current $I = 5$.

5.2. Two Line Sources

Now, we suppose that the cylinder is excited by two internal sources. According to the presentation of Section 4, for this problem there are six determinable parameters, namely $I_1, I_2, h_1, h_2, \phi_1$ and ϕ_2.

The procedure we follow is to formulate the system of (6), for $n = 0, \ldots, 5$, and solve it numerically to obtain the values of the above mentioned parameters. This system is solved in Matlab with the *lsqnonlin* function, which is a nonlinear least-squares solver using the trust-region-reflective algorithm. In such numerical algorithms, the choice of the initial vector has significant influence in the derived solutions. We investigate this systematically below.

First, we consider that the true parameters of the problem have the values $k_0 h_1 = 1$, $k_0 h_2 = 2, I_1 = 1, I_2 = 2, \phi_1 = \pi/3$ and $\phi_2 = \pi/5$ (these values do not correspond to the low-frequency regime). The cylinder's radius is selected as $k_0 a = 3$ and its refractive index as $n_1 = 2$. We denote the chosen initial vector in the numerical algorithm as $(I_1^0, I_2^0, k_0 h_1^0, k_0 h_2^0, \phi_1^0, \phi_2^0)$ and the vector of the true values as $(I_1, I_2, k_0 h_1, k_0 h_2, \phi_1, \phi_2) = (1, 2, 1, 2, 1.04719, 0.62831)$. Then, we define the relative deviations of the initial from the true values in the corresponding parameters as follows:

$$\tilde{d}(h_p) = \left| \frac{h_p - h_p^0}{h_p} \right|, \quad \tilde{d}(I_p) = \left| \frac{I_p - I_p^0}{I_p} \right|, \quad \tilde{d}(\phi_p) = \left| \frac{\phi_p - \phi_p^0}{\phi_p} \right|, \quad p = 1, 2.$$

Tables 3–8 depict the obtained values for the unknown parameters $k_0 h_1, k_0 h_2, I_1, I_2, \phi_1$ and ϕ_2, respectively, when each time the corresponding deviation of the initial from the true value $\tilde{d}(h_1), \tilde{d}(h_2), \tilde{d}(I_1), \tilde{d}(I_2), \tilde{d}(\phi_1)$ and $\tilde{d}(\phi_2)$ changes from 0 to 100%, while the deviations of all the other parameters are kept constant at values from 35% to 50%. In other words, in each Table, we change the deviation of the parameter that we determine from 0 to 100% and keep constant the deviations of all the other five parameters from 35% to 50%.

The conclusions from Tables 3–8 for the determination of each of the six unknown parameters are the following:

1. The coordinate h_1 of the first line source is determined quite accurately for all considered deviations. The maximum attained error in $k_0 h_1$ is 4.8%.
2. The coordinate h_2 of the second line source is determined accurately but only for deviations $\tilde{d}(h_2) \leq 60\%$ in which cases the error is (except from a single case) at

most 10%. Interestingly, the error is exactly zero for $\tilde{d}(h_2) \leq 40\%$ (again except from a single case).

3. The current I_1 of the first line source is determined very accurately. The error is exactly zero for all $\tilde{d}(I_1)$ and independently of the deviations of all the other parameters.
4. The accuracy in the determination of the current I_2 of the second line source is quite good but still deteriorated with respect to the corresponding one of I_1. The error for I_2 is exactly zero for the smaller deviations but reaches maximum levels of 25% for the larger ones.
5. The angle ϕ_1 of the first line source is determined with very small errors for all $\tilde{d}(\phi_1)$ (except from two cases) when the deviations of the other parameters are 35% and 40%. For the latter deviations being 45% and 50%, the error in ϕ_1 begins to attain large values.
6. For the determination of the angle ϕ_2 of the second line source, similar conclusions hold with respect to the previous ones for ϕ_1. Still, ϕ_2 seems to be affected more by the deviation of the initial from the true values.

Table 3. Computed values for the coordinate $k_0 h_1$ of the first line source when the deviation $\tilde{d}(h_1)$ of the initial from the true value of h_1 changes from 0 to 100% and the respective deviations of all the other five parameters are kept constant from 35% to 50%.

$\tilde{d}(h_1)$ (100%)	$\tilde{d}(h_2) = \tilde{d}(I_1) = \tilde{d}(I_2) = \tilde{d}(\phi_1) = \tilde{d}(\phi_2)$ (100%)			
	35	**40**	**45**	**50**
0	0.99795	0.95119	0.98824	0.95885
10	0.97213	0.98607	0.98776	0.99536
20	1.00000	1.00000	0.98818	0.98285
30	1.00000	1.00000	1.00000	0.98606
40	1.00000	1.00000	0.97328	0.98838
50	1.00000	0.99682	1.00000	0.97507
60	1.00000	0.98937	1.00000	0.98527
70	1.00000	0.99522	1.00000	0.98841
80	1.00000	0.97441	0.96578	0.97880
90	1.00000	0.97706	1.00000	1.00000
100	0.98818	0.95970	0.99148	0.98818

Table 4. Computed values for the coordinate $k_0 h_2$ of the second line source. The deviations in the parameters are as in Table 3.

$\tilde{d}(h_2)$ (100%)	$\tilde{d}(h_1) = \tilde{d}(I_1) = \tilde{d}(I_2) = \tilde{d}(\phi_1) = \tilde{d}(\phi_2)$ (100%)			
	35	**40**	**45**	**50**
0	2.00000	2.00000	2.00000	2.00000
10	2.00000	2.00000	2.00000	2.00000
20	2.00000	2.00000	2.00000	2.19844
30	2.00000	2.00000	2.00000	2.00000
40	2.00000	2.00000	2.00000	2.00000
50	2.02018	2.00000	2.20629	2.19184
60	2.00000	2.21465	2.65083	2.21188
70	2.24947	2.19718	4.19287	4.19287
80	3.70525	4.19287	4.19287	4.19287
90	5.69325	5.69325	5.69325	5.69325
100	4.83589	4.83589	4.83589	4.83589

Table 5. Computed values for the current I_1 of the first line source. The deviations in the parameters are as in Table 3.

$\tilde{d}(I_1)$ (100%)	$\tilde{d}(h_1) = \tilde{d}(h_2) = \tilde{d}(I_2) = \tilde{d}(\phi_1) = \tilde{d}(\phi_2)$ (100%)			
	35	**40**	**45**	**50**
0	1.00000	1.00000	1.21819	1.00000
10	1.00000	1.00000	1.19121	1.20396
20	1.00000	1.00000	1.13944	1.00000
30	1.00000	1.00000	1.13944	1.18869
40	1.00000	1.00000	1.18760	1.17616
50	1.00000	1.00000	1.20141	1.25820
60	1.00000	1.00000	1.20450	1.25896
70	1.00000	1.00000	1.01384	1.22971
80	1.00000	1.00000	1.00000	1.04399
90	1.00000	1.00000	1.00000	1.00000
100	1.00000	1.00000	1.22747	1.00000

Table 6. Computed values for the current I_2 of the second line source. The deviations in the parameters are as in Table 3.

$\tilde{d}(I_2)$ (100%)	$\tilde{d}(h_1) = \tilde{d}(h_2) = \tilde{d}(I_1) = \tilde{d}(\phi_1) = \tilde{d}(\phi_2)$ (100%)			
	35	**40**	**45**	**50**
0	2.00000	2.00000	2.00000	2.00000
10	2.00000	2.00000	2.47261	2.00000
20	2.00000	2.00000	2.00199	2.48470
30	2.00000	2.00000	2.00000	2.50198
40	2.00000	2.00000	2.49458	2.50944
50	2.00000	2.00000	2.48646	2.51300
60	2.00000	2.00000	2.46606	2.51253
70	2.00000	2.47396	2.46606	2.50552
80	2.00000	2.46606	2.46606	2.51088
90	2.00000	2.46606	2.47580	2.47156
100	2.48992	2.46606	2.48524	2.47732

Table 7. Computed values for the angle ϕ_1 of the first line source. The deviations in the parameters are as in Table 3.

$\tilde{d}(\phi_1)$ (100%)	$\tilde{d}(h_1) = \tilde{d}(h_2) = \tilde{d}(I_1) = \tilde{d}(I_2) = \tilde{d}(\phi_2)$ (100%)			
	35	**40**	**45**	**50**
0	1.04720	0.74056	0.60842	0.72143
10	1.04720	1.04705	1.03874	0.58387
20	1.04720	1.04720	0.55484	0.54910
30	1.04720	1.04720	0.57564	0.69884
40	1.04720	1.04720	1.04720	0.71457
50	1.04720	1.04720	0.64351	0.64562
60	1.04720	1.04720	1.04437	1.04242
70	1.04525	0.62998	1.04720	1.04720
80	1.04720	1.04720	1.04720	0.54910
90	1.04720	1.04720	1.04720	0.54910
100	1.04720	1.04720	1.04720	1.04720

Table 8. Computed values for the angle ϕ_2 of the second line source. The deviations in the parameters are as in Table 3.

$\tilde{d}(\phi_2)$ (100%)	$\tilde{d}(h_1) = \tilde{d}(h_2) = \tilde{d}(I_1) = \tilde{d}(I_2) = \tilde{d}(\phi_1)$ (100%)			
	35	**40**	**45**	**50**
0	0.62832	0.62832	0.62832	0.62832
10	0.62832	0.62832	0.62454	0.62832
20	0.62832	0.62832	0.62832	0.62832
30	0.62832	0.62832	0.62832	0.62832
40	0.62832	0.62832	0.62832	0.41308
50	0.62832	0.40347	0.62327	0.44134
60	0.62832	0.39645	0.62832	0.41863
70	0.62832	0.62832	0.62832	0.62832
80	0.62832	0.40532	0.45244	0.42789
90	0.62695	0.42719	0.39645	0.39953
100	0.35197	0.39645	0.44670	0.47905

As it has been shown above, some parameters of the problem are more and others are less sensitive to the deviations of the initial from the true values. However, in most cases even related deviations of up to 100% do in fact lead to acceptable results. For applications in which there are no a priori estimates for the values of the initial vector, additional investigations may be needed where one has to use and combine different methods of numerical analysis (not only the lsqnonlin function, which we implemented here). This can constitute an interesting future work direction.

Next, we examine the problem of determining the parameters of the two sources in the low-frequency regime. To this end, we consider a cylinder with $n_1 = 2$, $\mu_1 = 4$, and radius decreasing from $k_0 a = 1$ to $k_0 a = 0.0001$. The values of the currents of the two sources are $I_1 = 1$ and $I_2 = 2$, while the common angle of the sources is $\phi_0 = \pi/3$. For the radii of the sources, we consider that $h_1 = a/10$ and $h_2 = a/5$. The values of $k_0 h_1, k_0 h_2, I_1, I_2$ and ϕ_0 are computed be means of (8)–(11). The results are depicted in Table 9. It is evident that significantly accurate results are obtained for all five unknown parameters when $k_0 a = 0.01, 0.001, 0.0001$ in which cases the low-frequency assumption is certainly valid.

Table 9. Computed values for $k_0 h_1, k_0 h_2, I_1, I_2$ and ϕ_0 for $k_0 a = 1, 0.1, 0.01, 0.001, 0.0001$ when $h_1 = a/10$ and $h_2 = a/5$.

Parameters	$k_0 a$				
	1	**0.1**	**0.01**	**0.001**	**0.0001**
$k_0 h_1$	0.01049	0.01279	0.00101	0.00010	0.00001
$k_0 h_2$	0.13279	0.02079	0.00200	0.00020	0.00002
I_1	1.52156	1.47767	1.00829	1.00012	1.00000
I_2	5.22175	1.54421	1.99192	1.99988	2.00000
ϕ_0	0.64658	1.04246	1.04715	1.04719	1.04719

6. Conclusions

Two-dimensional inverse-source problems were considered corresponding to the excitation of a magnetodielectric cylinder by one or two internal line sources. We devised algorithms for the determination of the location coordinates and the currents of the sources. These algorithms relied on the calculation of the complex Fourier coefficients of the electric field on the cylindrical boundary. All the unknown parameters of the problem were determined by suitable manipulations of these coefficients. For the single-source inverse problem, the effect of noisy boundary data was investigated numerically. For the two-source problem, the nonlinear system for the unknown coefficients was solved either numerically or explicitly (the latter under the low-frequency assumption). The accuracy of the derived results was discussed in detail.

The algorithms presented in this work are mostly analytical in the sense that we try (in the cases where this is possible) to obtain explicit expressions for the problem's unknown parameters without resulting to a numerical solution or a numerical optimization scheme, e.g., to minimize some function as is a common approach in the existing literature. Furthermore, we point out that the developed algorithms are characterized by their simplicity and they can be considered in most cases as exact provided that the electric field on the cylinder is known exactly. In the case of inexact data, one needs to use some method to perform error analysis. Detailed work in this direction for acoustic problems has been presented in [27]. The origin of errors is from the measurements of the field on the cylinder and from numerical integration on the cylinder with the latter being potentially reduced by more accurate quadrature rules. The examined two-dimensional inverse problems are finite dimensional [12], since we aim to determine a set of numbers, such as the locations and currents of the line sources. For problems involving continuous distributions of sources, the methods discussed in this work are not directly applicable. Then, one has to result to other methods of a more numerical nature together with some optimization techniques, e.g., to determine the compact support of a continuous current distribution radiating inside a cylinder.

Interesting future work directions concern the extensions to finding line sources inside a two-layered circular cylinder or a homogeneous cylinder of elliptical cross section. Finally, referring to associated three-dimensional problems, determining the characteristics of two point sources or two point dipoles inside a spherical magneto-dielectric medium by extending the techniques of this work is also worth pursuing.

Author Contributions: Conceptualization, D.S.L. and N.L.T.; methodology, D.S.L. and N.L.T.; software, D.S.L.; formal analysis, D.S.L. and N.L.T.; investigation, D.S.L. and N.L.T.; writing—review and editing, D.S.L. and N.L.T. All authors have read and agreed to the published version of the manuscript.

Funding: This research received no external funding.

Data Availability Statement: Data supporting reported results are available from the authors upon reasonable request.

Conflicts of Interest: The authors declare no conflict of interest.

References

1. Isakov, V. *Inverse Source Problems*; American Mathematical Society Publications: Providence, RI, USA, 1990; ISBN 0821815326.
2. Fedeli, A.; Schenone, V.; Randazzo, A.; Pastorino, M.; Henriksson, T.; Semenov, S. Nonlinear S-Parameters Inversion for Stroke Imaging. *IEEE Trans. Microw. Theory Tech.* **2021**, *69*, 1760–1771. [CrossRef]
3. Senaratne, G.G.; Keam, R.B.; Sweatman, W.L.; Wake, G.C. Solutions to the Inverse Problem in a Two-Dimensional Model for Microwave Breast Tumour Detection. *Int. J. Intell. Syst. Technol. Appl.* **2007**, *3*, 133–148. [CrossRef]
4. Winges, J.; Cerullo, L.; Rylander, T.; McKelvey, T.; Viberg, M. Compressed Sensing for the Detection and Positioning of Dielectric Objects inside Metal Enclosures by Means of Microwave Measurements. *IEEE Trans. Microw. Theory Tech.* **2018**, *66*, 462–476. [CrossRef]
5. Alani, A.M.; Soldovieri, F.; Catapano, I.; Giannakis, I.; Gennarelli, G.; Lantini, L.; Ludeno, G.; Tosti, F. The Use of Ground Penetrating Radar and Microwave Tomography for the Detection of Decay and Cavities in Tree Trunks. *Remote Sens.* **2019**, *11*, 2073. [CrossRef]
6. Fedeli, A.; Pastorino, M.; Randazzo, A.; Gragnani, G.L. Analysis of a Nonlinear Technique for Microwave Imaging of Targets Inside Conducting Cylinders. *Electronics* **2021**, *10*, 594. [CrossRef]
7. Baratchart, L.; Ben Abda, A.; Ben Hassen, F.; Leblond, J. Recovery of pointwise sources or small inclusions in 2D domains and rational approximation. *Inverse Probl.* **2005**, *21*, 51–74. [CrossRef]
8. Ben Abda, A.; Ben Hassen, F.; Leblond, J.; Mahjoub, M. Sources recovery from boundary data: A model related to electroencephalography. *Math. Comput. Model.* **2009**, *49*, 2213–2223. [CrossRef]
9. Kandaswamy, D.; Blu, T.; Van De Ville, D. Analytic sensing: Noniterative retrieval of point sources from boundary measurements. *SIAM J. Sci. Comput.* **2009**, *31*, 3179–3194. [CrossRef]
10. Hanke, M.; Rundell, W. On rational approximation methods for inverse source problems. *Inverse Probl. Imaging* **2011**, *5*, 185–202. [CrossRef]
11. Abdelaziz, B.; Badia, A.E.; Hajj, A.E. Direct Algorithms for Solving Some Inverse Source Problems in 2D Elliptic Equations. *Inverse Probl.* **2015**, *31*, 105002. [CrossRef]

12. Tsitsas, N.L.; Martin, P.A. Finding a source inside a sphere. *Inverse Probl.* **2012**, *28*, 015003. [CrossRef]
13. Finke, S.; Gulrajani, R.M.; Gotman, J. Conventional and Reciprocal Approaches to the Inverse Dipole Localization Problem of Electroencephalography. *IEEE Trans. Biomed. Eng.* **2003**, *50*, 657–666. [CrossRef]
14. Lakhal, A.; Louis, A.K. Locating Radiating Sources for Maxwell's Equations Using the Approximate Inverse. *Inverse Probl.* **2008**, *24*, 045020. [CrossRef]
15. Pieper, K.; Tang, B.Q.; Trautmann, P.; Walter, D. Inverse Point Source Location with the Helmholtz Equation on a Bounded Domain. *Comput. Optim. Appl.* **2020**, *77*, 213–249. [CrossRef]
16. Alves, C.J.S.; Mamud, R.; Martins, N.F.M.; Roberty, N.C. On Inverse Problems for Characteristic Sources in Helmholtz Equations. *Math. Probl. Eng.* **2017**, 2472060. [CrossRef]
17. Liu, J.-C.; Li, X.-C. Reconstruction Algorithms of an Inverse Source Problem for the Helmholtz Equation. *Numer. Algorithms* **2020**, *84*, 909–933. [CrossRef]
18. Badia, A.E.; Nara, T. An Inverse Source Problem for Helmholtz's Equation from the Cauchy Data with a Single Wave Number. *Inverse Probl.* **2011**, *27*, 105001. [CrossRef]
19. Hamad, A.; Tadi, M. A Numerical Method for Inverse Source Problems for Poisson and Helmholtz Equations. *Phys. Lett. A* **2016**, *380*, 3707–3716. [CrossRef]
20. Saitoh, S. Inverse Source Problems in the Helmholtz equation. In *Inverse Problems and Related Topics*, 1st ed.; Nakamura, G., Saitoh, S., Kean, J.S., Eds.; Chapman & Hall/Crc: Boca Raton, FL, USA, 2000; ISBN 9781584881919.
21. Dassios, G. Electric and magnetic activity of the brain in spherical and ellipsoidal geometry. *Lect. Notes Math.* **2009**, *1983*, 133–202. [CrossRef]
22. Ammari, H. *An Introduction to Mathematics of Emerging Biomedical Imaging*; Springer: Berlin, Germany, 2008; ISBN 9783540795520.
23. Valagiannopoulos, C.A.; Tsitsas, N.L.; Fikioris, G. Convergence Analysis and Oscillations in the Method of Fictitious Sources Applied to Dielectric Scattering Problems. *J. Opt. Soc. Am. A* **2012**, *29*, 1–10. [CrossRef]
24. Kouroublakis, M.; Tsitsas, N.L.; Fikioris, G. Convergence Analysis of the Currents and Fields Involved in the Method of Auxiliary Sources Applied to Scattering by PEC Cylinders. *IEEE Trans. Electromagn. Compat.* **2021**, *63*, 454–462. [CrossRef]
25. Abramowitz, M.; Stegun, I.A. *Handbook of Mathematical Functions, with Formulas, Graphs, and Mathematical Tables*; Dover Publications: New York, NY, USA, 1965; p. 1046; ISBN 9780486612720.
26. Dassios, G.; Kleinman, R. *Low Frequency Scattering*; Oxford University Press: New York, NY, USA, 2000; ISBN 9780198536789.
27. Dassios, G.; Kamvyssas, G. Point source excitation in direct and inverse scattering: The soft and the hard small sphere. *IMA J. Appl. Math.* **1995**, *55*, 67–84. [CrossRef]